

PCAIM joint inversion of InSAR and ground-based geodetic time series: Application to monitoring magmatic inflation beneath the Long Valley Caldera

Yu-nung Nina Lin,¹ Andrew P. Kositsky,¹ and Jean-Philippe Avouac¹

Received 8 October 2010; accepted 26 October 2010; published 3 December 2010.

[1] This study demonstrates the interest of using a Principal Component Analysis-based Inversion Method (PCAIM) to analyze jointly InSAR and ground-based geodetic time series of crustal deformation. A major advantage of this approach is that the InSAR tropospheric biases are naturally filtered out provided they do not introduce correlated or high amplitude noise in the input times series. This approach yields source models which are well-constrained both in time and space due to the temporal resolution of the ground-based geodetic data and the spatial resolution of the InSAR data. The technique is computationally inexpensive allowing for the inversion of large datasets. To demonstrate the performance of this approach, we apply it to the 1997–98 magmatic inflation event in the Long Valley Caldera, California. **Citation:** Lin, Y. N., A. P. Kositsky, and J.-P. Avouac (2010), PCAIM joint inversion of InSAR and ground-based geodetic time series: Application to monitoring magmatic inflation beneath the Long Valley Caldera, *Geophys. Res. Lett.*, 37, L23301, doi:10.1029/2010GL045769.

1. Introduction

[2] A number of ground-based geodetic techniques and remote sensing techniques are now available to monitor surface deformation induced by a variety of geophysical processes and are used to address a wide range of questions in various fields [e.g., *Blewitt, 2007; Simons and Rosen, 2007*]. Some ground-based geodetic techniques, such as Electronic Distance Meter (EDM) and Global Positioning System (GPS), allow high temporal resolution, with sampling rates typically between more than 1 measurement epoch per second and 1 measurement epoch every several days. These measurements are based on electromagnetic signals transmitted through the atmosphere between pairs of ground-based stations or between ground-based stations and satellites, and are therefore sensitive to atmospheric effects. Atmospheric effects are routinely estimated and corrected for in processing continuous GPS data [*Tregoning and Herring, 2006; Blewitt, 2007*] and EDM data [*Langbein et al., 1987*]. Therefore, such post-corrected time series are relatively free of atmospheric bias.

[3] While ground-based geodetic techniques provide dense time series of accurate positions at a limited number of points, remote sensing techniques, in particular Interferometric Synthetic Aperture Radar (InSAR), can provide

dense spatial coverage, but at a limited number of epochs, given that the revisit period of most SAR systems is 10–50 days. Another issue is the sensitivity of InSAR to atmospheric disturbances, particularly moisture variations in the troposphere. Various methods have been proposed to correct these effects [e.g., *Li et al., 2005, 2006; Foster et al., 2006; Onn and Zebker, 2006; Puysségur et al., 2007; Doin et al., 2009; Lin et al., 2010*], but the potential of these techniques is limited by the availability of radiometric data, the density of GPS stations, or the accuracy of high-resolution weather models. Difficulties in correcting atmospheric influences, in addition to the generally long time span between interferometric pairs of images, strongly limit the possibility of using InSAR to monitor the temporal variation of surface deformation.

[4] Because of the complementary resolution of InSAR and ground-based geodetic data, geophysical analyses can benefit from integrating both types of data into the same inversion [e.g., *Wei et al., 2010*]. Here we explore the possibility of achieving this goal using the Principal Component Analysis-based Inversion Method (PCAIM) [*Kositsky and Avouac, 2010*]. PCAIM is a statistically-based approach to extract the signals with maximum spatiotemporal coherence and derive a best fitting source model with minimum computational cost. In the standard PCA approach the first principal component is the least squares approximation of the data matrix; the second principal mode is the best approximation of the residuals after subtracting the first principal component from the data matrix; and so forth [*Savage, 1988*]. PCAIM takes additional advantage of the fact that the components can be modeled separately and that the derived principal sources can be recombined to derive the best fitting time-varying source model. Because tectonics must affect both the ground-based geodetic and InSAR time series in a coherent way, while atmospheric delays ought not, this technique utilizes ground-based geodetic data to help filter out InSAR tropospheric biases. The two datasets also complement each other in terms of spatiotemporal sampling rates in the PCAIM output. In this study, we use the Long Valley Caldera example to test this joint inversion method. Long Valley Caldera experienced a large inflation episode between 1997 and 1998, resulting in ~10 cm of cumulative uplift [*Langbein, 2003*]. Hereafter we show how to derive a source model with high spatiotemporal resolution from the joint inversion of InSAR and ground-based geodetic data.

2. Joint Inversion Using PCAIM

2.1. PCAIM Principles

[5] Provided that the crust is considered as a linear elastic medium, surface displacements data depend linearly on the source characteristics, typically parameterized as slip on a

¹Division of Geological and Planetary Sciences, California Institute of Technology, Pasadena, California, USA.

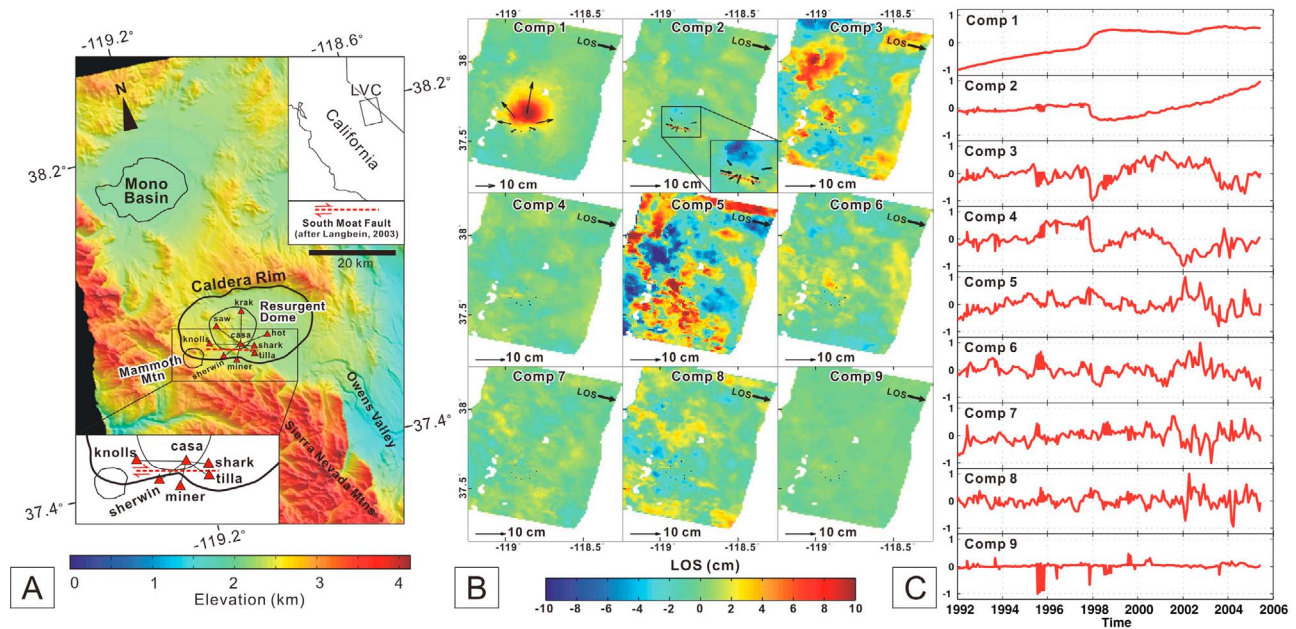


Figure 1. (a) Reference map of Long Valley Caldera and the resurgent dome during the 1997–98 inflation episode. This map has the same extent as the data footprint of ERS track 485 used in this study. Lower left inset shows the inferred location of the South Moat Fault [Langbein, 2003]. The results from PCA decomposition. (b) The spatial functions of the displacement field, multiplied with the principal values associated with each component. Arrows in each component represent the principal slip functions (relative to CASA) associated with each EDM station. Notice that the inset in the 2nd component is on a different color scale for visualization purpose. (c) The corresponding time functions. The first two components show primarily tectonic signals although the spatial function associated with the 2nd component also shows signs of tropospheric effects.

fault, opening of a dike or increase in pressure in a magmatic chamber [e.g., Mogi, 1958; Okada, 1985]. Source models can therefore be derived, through some standard linear inversion procedure. In principle, the time evolution of the source can be derived from inverting the displacement data available at each epoch. Such an approach is computationally expensive for large dataset, and would not impose any coherent time evolution of the source since it would yield independent models at each epoch. PCAIM allows us to overcome these limitations. The displacement data are decomposed into a linear combination of *principal components*, each associated with its own spatial function, principal value and time function. Kositsky and Avouac [2010] have shown that if the dataset can be modeled as a time-varying linear source model, the principal spatial functions can be modeled using the same formalism. After PCA (Principal Component Analysis) decomposition, each principal spatial function is modeled individually and translated into a corresponding principal source model. The various principal source models are then recombined with their respective principal values and time functions to represent the estimate of the source model needed to fit the original dataset. PCAIM thus takes advantage of the linearity of the formulation and is cost effective because it generally requires inversion of only a handful of spatial components. For more details regarding the theoretical and technical aspects of this method, the reader can refer to Kositsky and Avouac [2010].

2.2. PCA Decomposition

[6] We use a total of 65 interferograms formed from 24 ERS scenes acquired between 1992 and 2005, and two-

color EDM records acquired every 1–15 days since January 1984 (Figure 1a). We applied a standard small baseline subset (SBAS) time series analysis [Berardino *et al.*, 2002] on the InSAR data, without any correction terms or additional filtering. The SBAS InSAR time series consist of 24 epochs on 7992 pixels (1-km spacing), with median time span of 70 days between epochs. The EDM time series consist of 185 epochs at 8 stations. These two datasets were combined into one large displacement data matrix, which is zero-padded in most entries due to the low temporal sampling rate of SAR imagery. Ordinary PCA cannot be applied to such sparse matrices. To get around this problem, we adopt a more sophisticated decomposition, a non-linear solver using the weighted low-rank approximation originally developed by Srebro and Jaakkola [2003] and adapted to geodetic applications by Kositsky [2010]. The method thus allows taking into account the formal uncertainties assigned to the data and is therefore more practical than the standard PCA technique when the time series have missing data and/or varying uncertainties [Kositsky and Avouac, 2010].

[7] Another adaptation is that each component is solved separately in order to preserve the continuity of time functions. This iterative decomposition strategy retains the signal continuity of each component (see auxiliary material).¹ The resultant principal components are close to but not exactly orthogonal. Nevertheless, orthogonality is not geophysically necessary, whereas temporal continuity is. To maintain the

¹Auxiliary materials are available in the HTML. doi:10.1029/2010GL045769.

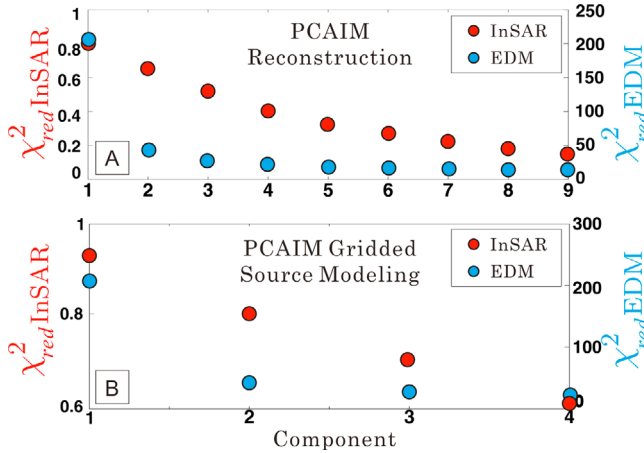


Figure 2. Graphs showing the changes of χ_r^2 of the residuals (a) between the observed and reconstructed time series and (b) between the observed and modeled times series as the number of components increases. χ_r^2 is computed considering either the InSAR or the EDM data separately according to equation (1). The closer χ_r^2 is to one, the closer the estimated errors are to the observational/assigned uncertainties, and hence the result is considered to be more reasonable.

continuity of time functions, we think it is an acceptable tradeoff with the cost of orthogonality. Figures 1b and 1c show the spatial functions, multiplied by the principal values associated with each component, and the normalized time functions.

[8] Figure 2a shows how the fit between the original times series and the reconstructed time series improves as the number of components used in the reconstruction increases. Here, we consider separately the reduced Chi-square χ_r^2 of the residuals to the EDM and to the InSAR data for the 1 to k -th component, defined as,

$$\chi_{r\ TYPE}^2 = \frac{1}{N - P} \sum_{i=1}^k \left[\frac{X_{TYPE}^{obs} - X_{TYPE}^{pca}}{\sigma_{TYPE}^{obs}} \right]^2 \quad (1)$$

where N and P refers to the total number of data and parameters respectively, X refers to data matrix, TYPE refers either to InSAR or EDM, and σ is the formal 1-sigma uncertainties assigned to the data. For the EDM data we used the original uncertainties from Langbein [2003]. For the InSAR data we used a standard estimate of 5 mm, ignoring the off-diagonal elements of the variance-covariance uncertainty matrix. Figure 2a shows that with only the 1st component, the InSAR data can be reconstructed within the 5 mm estimated uncertainty. Under the same χ_r^2 criterion, it takes more than 10 components to fit the EDM data within their original uncertainties. It is thus difficult to determine the overall number of significant components because of the sensitivity of χ_r^2 to the observational/assigned uncertainty. In this situation, F -test serves as a more robust approach. This statistical test estimates the probability that a particular component be significant based on the relative reduction of variance (χ_r^2 in fact) as this component is added. The test result indicates that 3 components are significant at the 95% confidence level to reconstruct the EDM data (Table S1 of

the auxiliary material). More components are needed for InSAR because higher order components account for the atmospheric noises that prevail in all interferograms.

2.3. Results of the Joint Inversion

[9] We chose a source model consisting of a grid of point volume-sources in an elastic half space [Masterlark and Lu, 2004], and compute the Green's functions accordingly. The gridded source has dimensions of 110 km by 125 km by 20 km, with distribution of 5 km spacing in X and Y direction and 2 km spacing in Z direction. We applied regularization via imposing a penalty to roughness of the source model, and carried out cross-validation to determine the optimal value for the smoothing parameter. The χ_r^2 of the residuals between the observed times series and the predictions from the gridded source model shows decreasing trends as the number of components increases (Figure 2b), but still gives no clue to where the cut-off component is. We therefore applied F -test again (Table S1), and found that the first 2 components are significant at the 95% confidence level with regard to the fit to the original EDM data. More than 4 components are needed for the InSAR data because including higher-order components into the model improves the fitting to the prevailing noises in the data. Since the EDM dataset is less influenced by atmospheric noise and hence its F -test will be less biased, we chose to use only 2 components to generate our final model. The first 2 principal volumes are then recombined with their time functions to generate the time varying source model that best fits jointly the InSAR and EDM data, without being significantly biased by the tropospheric noise in the InSAR data (Figure 3; see auxiliary material for Animations S1–S4).

[10] The EDM time series are generally well-reproduced by the model obtained from the inversion of the first 2 components, except for the station MINER and TILLA (Figure 3a). These two stations lie along the southern flank of the caldera (Figure 1a). According to Langbein [2003], the southern flank is subject to the influence of the South Moat Fault, a right-lateral strike-slip fault dipping 70 degree to the NE. MINER and TILLA should have recorded the deformation associated with the displacement on this fault, and so does the InSAR imagery as the pattern is visible in the spatial function of the 2nd component (Figure 1b). For the purpose of demonstration, we did not include this fault so that it is easier to keep track of the roles InSAR and EDM data play in one single source model, but one can certainly include multiple types of sources in PCAIM.

3. Discussion and Conclusion

[11] Our source model suggests inflation of a magma chamber close to a sphere centered at around 7–8 km, similar to the 7.5 km centroid depth estimated by Langbein [2003]. The net increase of volume over the period of time analyzed here is estimated to 0.02 km³, a value slightly smaller than the (~0.03 km³) estimate of Langbein [2003]. It should be noticed that the gridded point inflation source model is a purely kinematic description of the magmatic source; as such it does not necessarily satisfy the traction-free boundary condition of the prolate spheroid model of Yang *et al.* [1988]. In fact, PCAIM only requires the surface displacement to be a linear function of the source model parameters, and the source model itself to be linear so that it

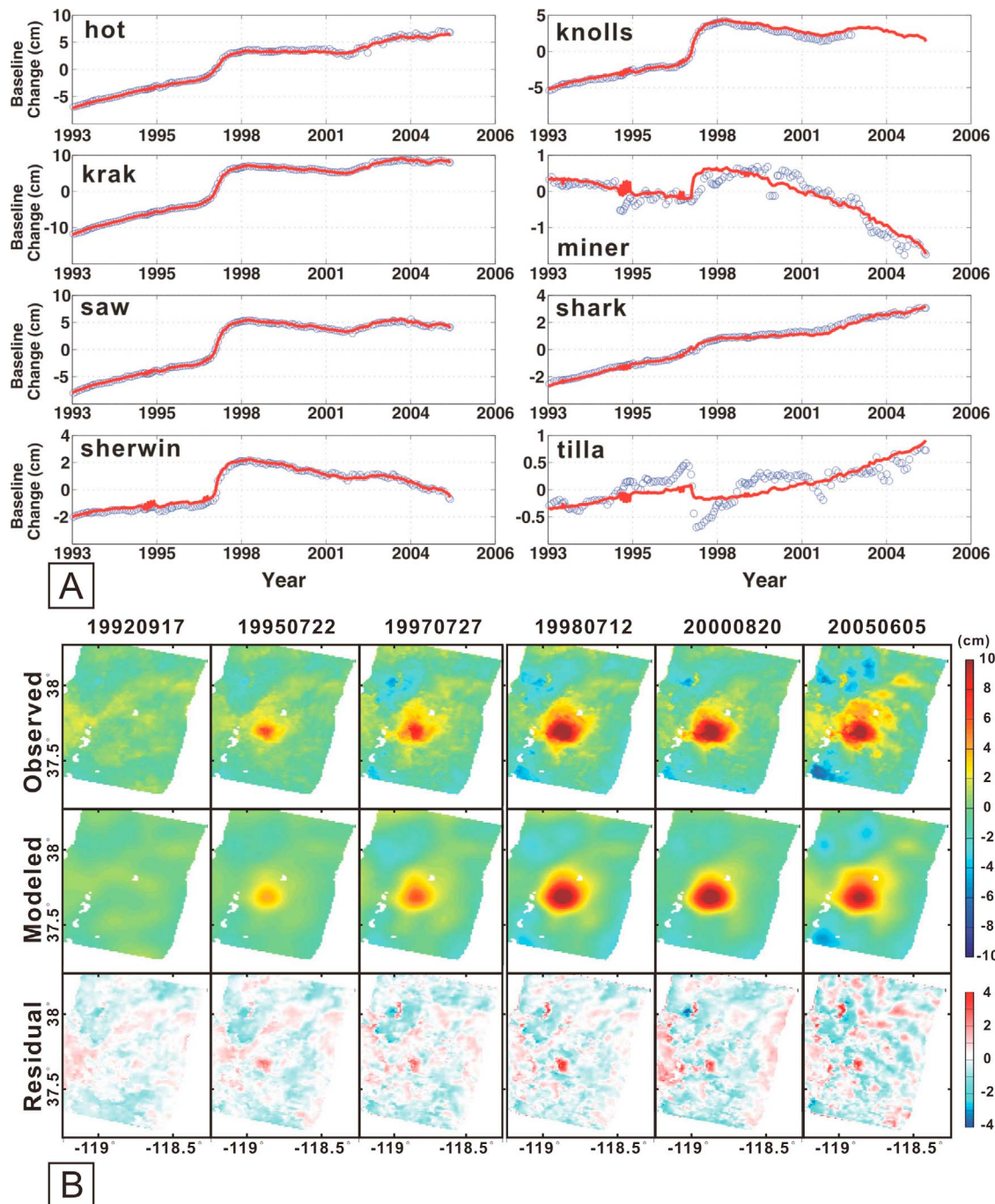


Figure 3. (a) Comparison between the observed and modeled EDM time series. The misfits are small at most stations but larger at station MINER and TILLA, probably due to the proximity of these stations to the South Moat fault, which is not taken into account in our modeling. Note the amplitude of the geodetic signals at these two stations is also way smaller than at all the other stations. (b) Upper plot shows the observed InSAR time series of cumulative deformation and the model predictions computed from the inversion of the first 2 components. All time steps are relative to the first date of the SBAS time series (19920604). Only selected time snapshots are shown in this plot. Lower plot shows the residual. Some noises in the 2nd component are captured when doing inversion, but in general there is no significant tectonic signal left in the residual plots. These plots show that the first 2 components are sufficient to account for most of the tectonic signals in the datasets.

conforms to the principles of additivity and scaling. In this sense there is no theoretical difficulty using the prolate spheroid model [Yang *et al.*, 1988] and including the South Moat Fault in a PCAIM joint inversion.

[12] Our study demonstrates that PCAIM is an effective tool to separate tectonic signals and noises into different

components when EDM and InSAR data are analyzed jointly. Most tectonic signals are in the first component and some are in the second component, while the third and higher components are dominated by tropospheric effects or tectonic sources too weak to have induced significantly correlated and high-amplitude signals in the whole dataset

analyzed here (Figure 1). We discuss in the auxiliary material the results obtained from the decomposition of the InSAR-only or the EDM-only data. They show that joint analysis of the EDM and InSAR indeed helps extract from the 1st and 2nd components the fraction of the InSAR signals that are not coherent with EDM data. The joint inversion allows better spatial constraints and less-biased temporal evolution history to the source model.

[13] Low-amplitude transient signals may be mixed with short-timescale tropospheric noises into higher order components. The EDM data from station MINER and TILLA show indeed a short-lived transient that is very likely tectonic signal. This transient was captured into the InSAR-dominant spatial function but unfortunately mixed with tremendous tropospheric noises. This is a limitation of PCAIM: when high-amplitude noise exists, corresponding corrections (if available) must be carried out, otherwise small-amplitude signals at a small number of measurement locations will blend with noise in higher order components.

[14] The final remark about PCAIM is its low computational cost: it takes only ~2–3 hours to invert the whole dataset used in this study on a standard Linux machine (2.4 GHz CPU). The PCAIM code and sample dataset is available from the Tectonics Observatory Web page (<http://www.tectonics.caltech.edu/resources/pcaim/>).

[15] **Acknowledgments.** We thank Mark Simons for providing the SAR data used in this study. APK thanks Tapio Schneider for helpful conversations. This research was partially funded by the Gordon and Betty Moore Foundation and by the Keck Institute of Space Studies. It is Caltech Tectonics Observatory contribution 137.

References

- Berardino, P., G. Fornaro, R. Lanari, and E. Sansosti (2002), A new algorithm for surface deformation monitoring based on small baseline differential SAR interferograms, *IEEE Trans. Geosci. Remote Sens.*, *40*, 2375–2383.
- Blewitt, G. (2007), GPS and space-based geodetic methods, in *Treatise on Geophysics*, vol. 3, *Geodesy*, edited by G. Schubert, pp. 351–390, Elsevier, Amsterdam.
- Doin, M. P., C. Lasserre, G. Peltzer, O. Cavalie, and C. Doubre (2009), Corrections of stratified tropospheric delays in SAR interferometry: Validation with global atmospheric models, *J. Appl. Geophys.*, *69*, 35–50, doi:10.1016/j.jappgeo.2009.03.010.
- Foster, J., B. Brooks, T. Cherubini, C. Shacat, S. Businger, and C. L. Werner (2006), Mitigating atmospheric noise for InSAR using a high resolution weather model, *Geophys. Res. Lett.*, *33*, L16304, doi:10.1029/2006GL026781.
- Kositsky, A. (2010), PCAIM user's manual, Calif. Inst. of Technol., Pasadena. (Available at <http://www.tectonics.caltech.edu/resources/pcaim/>)
- Kositsky, A. P., and J.-P. Avouac (2010), Inverting geodetic time series with a principal component analysis-based inversion method, *J. Geophys. Res.*, *115*, B03401, doi:10.1029/2009JB006535.
- Langbein, J. (2003), Deformation of the Long Valley Caldera, California: Inferences from measurements from 1988 to 2001, *J. Volcanol. Geotherm. Res.*, *127*, 247–267, doi:10.1016/S0377-0273(03)00172-0.
- Langbein, J., M. Linker, and D. Tupper (1987), Analysis of two-color geodimeter measurements of deformation within the Long Valley Caldera: June 1983 to October 1985, *J. Geophys. Res.*, *92*(B9), 9423–9442.
- Li, Z., J.-P. Muller, P. Cross, and E. J. Fielding (2005), Interferometric synthetic aperture radar (InSAR) atmospheric correction: GPS, Moderate Resolution Imaging Spectroradiometer (MODIS), and InSAR integration, *J. Geophys. Res.*, *110*, B03410, doi:10.1029/2004JB003446.
- Li, Z., J.-P. Muller, P. Cross, P. Albert, J. Fischer, and R. Bennartz (2006), Assessment of the potential of MERIS near-infrared water vapour products to correct ASAR interferometric measurements, *Int. J. Remote Sens.*, *27*, 349–365, doi:10.1080/01431160500307342.
- Lin, Y. N., M. Simons, E. A. Hetland, P. Muse, and C. DiCaprio (2010), A multiscale approach to estimating topographically correlated propagation delays in radar interferograms, *Geochem. Geophys. Geosyst.*, *11*, Q09002, doi:10.1029/2010GC003228.
- Masterlark, T., and Z. Lu (2004), Transient volcano deformation sources imaged with interferometric synthetic aperture radar: Application to Segum Island, Alaska, *J. Geophys. Res.*, *109*, B01401, doi:10.1029/2003JB002568.
- Mogi, K. (1958), Relations between the eruption of various volcanoes and the deformation of the ground surface around them, *Bull. Earthquake Res. Inst. Univ. Tokyo*, *36*, 99–143.
- Okada, Y. (1985), Surface deformation due to shear and tensile faults in a half-space, *Bull. Seismol. Soc. Am.*, *75*(4), 1135–1154.
- Onn, F., and H. A. Zebker (2006), Correction for interferometric synthetic aperture radar atmospheric phase artifacts using time series of zenith wet delay observations from a GPS network, *J. Geophys. Res.*, *111*, B09102, doi:10.1029/2005JB004012.
- Puysségur, B., R. Michel, and J.-P. Avouac (2007), Tropospheric phase delay in interferometric synthetic aperture radar estimated from meteorological model and multispectral imagery, *J. Geophys. Res.*, *112*, B05419, doi:10.1029/2006JB004352.
- Savage, J. C. (1988), Principal component analysis of geodetically measured deformation in Long Valley Caldera, eastern California, 1983–1987, *J. Geophys. Res.*, *93*(B11), 13,297–13,305.
- Simons, M., and P. Rosen (2007), Interferometric synthetic aperture radar geodesy, in *Treatise on Geophysics*, vol. 3, *Geodesy*, edited by G. Schubert, pp. 391–446, Elsevier, Amsterdam.
- Srebro, N., and T. Jaakkola (2003), Weighted low-rank approximations, in *Proceedings of the Twentieth International Conference on Machine Learning*, pp. 720–727, AAAI Press, Menlo Park, Calif.
- Tregoning, P., and T. A. Herring (2006), Impact of a priori zenith hydrostatic delay errors on GPS estimates of station heights and zenith total delays, *Geophys. Res. Lett.*, *33*, L23303, doi:10.1029/2006GL027706.
- Wei, M., D. Sandwell, and B. Smith-Konter (2010), Optimal combination of InSAR and GPS for measuring interseismic crustal deformation, *Adv. Space Res.*, *46*(2), 236–249, doi:10.1016/j.asr.2010.03.013.
- Yang, X.-M., P. M. Davis, and J. H. Dieterich (1988), Deformation from inflation of a dipping finite prolate spheroid in an elastic half-space as a model for volcanic stressing, *J. Geophys. Res.*, *93*(B5), 4249–4257.

J.-P. Avouac, A. P. Kositsky, and Y. N. Lin, Division of Geological and Planetary Sciences, California Institute of Technology, MC 100-23, 1200 E. California Blvd., Pasadena, CA 91125, USA. (ninalin@caltech.edu)